This is a preprint, the final version is subject to change, of the American Mineralogist (MSA)
Cite as Authors (Year) Title. American Mineralogist, in press.
(DOI will not work until issue is live.) DOI: http://dx.doi.org/10.2138/am.2014.4407

Revision 2

The system K_2CO_3-$MgCO_3$ at 6 GPa and 900-1450 ºC

Anton Shatskiy[1,2*], Igor S. Sharygin[1,2], Pavel N. Gavryushkin [1,2], Konstantin D. Litasov[1,2], Yuri M. Borzdov[1], Anastasia V. Shcherbakova[3], Yuji Higo[4], Ken-ichi Funakoshi[4], Yuri N. Palyanov[1,2], Eiji Ohtani[5].

[1]V.S. Sobolev Institute of Geology and Mineralogy, Russian Academy of Science, Siberian Branch, Koptyuga pr. 3, Novosibirsk 630090, Russia

[2]Novosibirsk State University, Novosibirsk 630090, Russia

[3]John and Willie Leone Family Department of Energy and Mineral Engineering, Penn State University, University Park 16802, USA

[4]Japan Synchrotron Radiation Research Institute, SPring-8, Kouto, Hyogo 678-5198, Japan

[5]Department of Earth and Planetary Material Science, Tohoku University, Sendai 980-8578, Japan

Abstract

Phase relations in the K_2CO_3-$MgCO_3$ system have been studied in high-pressure high-temperature (HPHT) multianvil experiments using graphite capsules at 6.0±0.5 GPa pressures and 900-1450 °C temperatures. Subsolidus assemblies comprise the fields K_2CO_3 + $K_2Mg(CO_3)_2$ and $K_2Mg(CO_3)_2$ + $MgCO_3$ with the transition boundary near 50 mol% $MgCO_3$ in the system. The K_2CO_3-$K_2Mg(CO_3)_2$ eutectic is established at 1200 ºC and 25 mol% $MgCO_3$. Melting of K_2CO_3 occurs between 1400 and 1450ºC. We propose that $K_2Mg(CO_3)_2$ disappears between 1200 and 1300 ºC via congruent

melting. Magnesite is observed as a subliquidus phase to temperatures in excess of 1300 ºC.

At 6 GPa, melting of the $K_2Mg(CO_3)_2 + MgCO_3$ assemblage can be initiated either by heating to 1300 ºC under "dry" conditions or by adding a certain amount of water at 900-1000 °C. Thus, the $K_2Mg(CO_3)_2$ could control the solidus temperature of the carbonated mantle under "dry" conditions and cause formation of the K- and Mg-rich carbonatite melts similar to those found as microinclusions in "fibrous" diamonds.

The $K_2Mg(CO_3)_2$ compound was studied using *in situ* X-ray coupled with a DIA-type multianvil apparatus. At 6.5 GPa and 1000 °C, the structure of $K_2Mg(CO_3)_2$ was found to be orthorhombic with lattice parameters a = 8.8898(7), b = 7.8673(7) and c = 5.0528(5), V = 353.39(4). No structure change was observed during pressure decrease down to 1 GPa. However, recovered $K_2Mg(CO_3)_2$ exhibited a trigonal $R\bar{3}m$ structure previously established at ambient conditions.

Introduction

Alkalis (Na, K) and carbonates play a key role in diamond formation (Schrauder and Navon 1994; Pal'yanov et al. 1999a, 2002, 2007), mantle metasomatism (Green and Wallace 1988; Haggerty 1989), and deep magma generation (Wallace and Green 1988; Sweeney 1994; Dobretsov and Shatskiy 2012). They are major components of carbonatite melts entrapped by mantle minerals such as "fibrous" diamonds and olivines from kimberlite pipes (Navon 1991; Izraeli et al. 2004; Tomlinson et al. 2006; Golovin et al. 2007; Klein-BenDavid et al. 2009; Korsakov et al. 2009; Logvinova et al. 2011; Sharygin et al. 2013; Weiss et al. 2009; Zedgenizov et al. 2011). Experimental data on the conditions under which K enters the pyroxene structure (Harlow 1997) leads us to hypothesize that clinopyroxenes from inclusions

in diamonds and diamond-bearing metamorphic rocks with up to 1 wt% K_2O (Sobolev et al. 1972; Sobolev and Shatsky 1990; Harlow and Veblen 1991; Sobolev et al. 1991; Shatsky et al. 1995) are crystallized from ultrapotassic carbonate-silicate melts containing 15-28 wt% K_2O. Numerous mantle xenoliths from different localities display the petrographic and geochemical signatures of carbonatite metasomatism (Yaxley et al. 1991; Shatsky et al. 2008). Alkali carbonates would be essential components, which control melting in subducting slab and upwelling mantle. Minor amounts of alkalis and CO_2 drastically reduce, by ~1000 °C, the solidus of lithospheric mantle and subducted rocks (peridotites, eclogites, and pelites (Brey et al. 2011; Grassi and Schmidt 2011; Litasov 2011)). Melting at 3-21 GPa yields alkali-rich Ca-Mg carbonate melts (Litasov et al. 2013). It has been shown experimentally that kimberlitic magma should have an alkali-rich carbonatite composition under conditions existing in the lithospheric mantle (Litasov et al. 2010; Sharygin et al. 2013). It is thus essential to understand phase relations in simple alkali-alkaline earth carbonate systems under mantle conditions. As part of an investigation of those systems, K_2CO_3-$MgCO_3$ has a particular importance, due to the abundance of K and Mg in carbonatite melts from continental sublithospheric mantle entrapped by diamonds (Schrauder and Navon 1994; Klein-BenDavid et al. 2009; Zedgenizov et al. 2009).

The K_2CO_3-$MgCO_3$ system (Data and Tuttle 1964; Sharma and Simons 1980; Simons and Sharma 1982; Genge et al. 1995), has been studied previously at $P(CO_2)$ = 0.0034 GPa (Eitel and Skaliks 1929) and 0.1 GPa (Ragone et al. 1966). Studies showed that a $K_2Mg(CO_3)_2$ compound, with space group $R\bar{3}m$, is stable in this system at lower temperatures, near 300 ºC and at pressures of 0.025 GPa (Hesse and Simons 1982), but it is replaced with the K_2CO_3 + $MgCO_3$ assemblage at higher temperatures.

In this paper, we present experimental data on phase relations in the system K_2CO_3-$MgCO_3$ at 6 GPa and 900-1450 ºC under nominally "dry" and hydrous conditions and highlight our results of *in situ* X-ray diffraction of the $K_2Mg(CO_3)_2$ compound at high pressure.

Experimental methods

In this study we have conducted three sets of HP-HT multianvil experiments: Kawai experiments to study phase relations in the K_2CO_3-$MgCO_3$ system, BARS experiments (a transliteration of a Russian abbreviation of a pressless split-sphere apparatus) along the K_2CO_3-hydromagnesite join to examine the effect of water on the phase relations in the K-Mg carbonate system, and X-ray diffraction (XRD) experiments to identify the $K_2Mg(CO_3)_2$ crystal structure *in situ* at HPHT conditions. Below we present the details of each set of experiments.

Kawai experiments were performed using 3000- and 1500-ton presses with DIA- (Osugi et al. 1964) and wedge-type guide blocks (Lloyd et al. 1963; Kawai et al., 1973) at Tohoku University (Sendai, Japan). We chose Ca-doped ZrO_2 ceramics as the pressure medium (PM) (Fig. 1), the material specification of which is given in Shatskiy et al. (2010a). The ZrO_2 ceramics were shaped as 20.5-mm octahedra with ground edges and corners, fired with other ceramic parts at 950 °C for 2 hours and than stored in a drying oven prior to cell assembly preparation. The high-pressure cell was compressed by 12-mm anvil truncations. We used unfired pyrophyllite gaskets, 4.0 mm in both width and thickness to seal the compressed volume and support the anvil flanks.

Room-temperature pressure calibration of a given cell was performed for both DIA- and wedge-type apparatuses by monitoring the resistance changes in Bi at 2.5

GPa and 7.7 GPa (Decker et al. 1972) and Ba at 5.5 GPa (Haygarth et al. 1967) using the four-wire method (Shatskiy et al. 2011). Ba wire was covered by a Si-based vacuum grease to prevent its oxidation. Pressure calibration at HT was carried out using known phase transitions in SiO_2 (quartz-coesite) at 1100 °C (Bohlen and Boettcher 1982) and $CaGeO_3$ at 1100 °C (Ono et al. 2011) (Fig. 2). Deviation of pressure from the desirable value during heating to 900-1500 °C in the given cell and press load did not exeed ± 0.5 GPa, as confirmed by *in situe* X-ray diffraction experiments at the BL04B1 beamline of the SPring-8 synnhrotron radiation facility.

The design of the cell assemblage is shown in Figure 1a. The cell assembly contains four graphite cassettes (i.e., multiple sample holders). Each cassette contains four holes. To study the present system we used two upper cassettes (i.e. eight holes with different sample compositions shown in Table 1). The remaining holes were employed to study alternative carbonate systems. Neighboring compositions were loaded in different cassettes to avoid systematic error related to thermal gradients, e.g. 90, 60, 40, 20 mol% K_2CO_3 in the lower high-temperature (HT) cassette and 75, 50, 30, 10 mol% K_2CO_3 in the upper low-temperature (LT) cassette. Graphite heater, 4.5/4.0 mm in outer/inner diameter and 11 mm in length, was used to heat samples. A WRe(3/25) thermocouple was inserted in the center of the PM, through the heater walls and electrically insulated by Al_2O_3 tubes. No correction was made for the effect of pressure on the thermocouple electromotive force. Maximum radial and axial thermal gradients across the sample charges were examined using a two-pyroxene thermometer (Brey and Kohler 1990) and thermal modeling software (Hernlund et al. 2006) and were found to be about 5 and 10°C/mm, respectively (Fig. 3). Thus, the maximum temperature difference between samples did not exceed 20 °C.

Mixtures of synthetic K_2CO_3 and natural magnesite from Bahia, Brazil, with a composition of $Mg_{0.975}Fe_{0.015}Mn_{0.006}Ca_{0.004}CO_3$ were used as starting materials. The mixtures were ground in an agate mortar under acetone and loaded as a powder into the cassettes. The loaded cassettes were dried at 300ºC for 3-5 hours and stored in a drying oven. Prepared assemblies were stored at 130ºC in a vacuum for ≥12 hours prior to experiment. During opening the vacuum oven was filled with dry air from a drying oven.

All experiments were performed as follows: the assemblies were compressed at room temperature to 6.0 MN (600 ton) in a DIA press, or to 4.5 MN (450 ton) in a wedge press, corresponding to a pressure of 6 GPa. Then the samples were heated to temperatures ranging from 900 to 1400 °C for 1-43 hours. The temperature was maintained within 0.5 °C of the desired value using the temperature controlling program (written by T. Katsura). Experiments were terminated by turning off the electrical power to the heater, followed by slow decompression.

BARS experiments were carried out using a pressless split-sphere apparatus (BARS) developed in IGM SB RAS (Novosibirsk, Russia) (Malinovskii et al. 1989; Palyanov et al. 1990; Palyanov et al. 2010). We employed ZrO_2-based ceramics as a PM shaped into a tetragonal prism (20.4×20.4×25.2 mm). The PM was compressed by two anvils with 18×18 mm square truncations and four anvils with 18×23 mm rectangular truncations. The sample pressure was controlled by varying the oil pressure in the hydraulic system of the BARS apparatus. Sample heating was achieved using a tubular graphite heater, 13.0/12.0 mm in outer/inner diameter and 19.0 mm in height. The sample temperature was controlled using a PtRh(6/30) thermocouple. Mixtures of synthetic K_2CO_3 and hydromagnesite, $Mg_5(CO_3)_4(OH)_2 \cdot 4H_2O$, were used as starting materials (Table 2). The mixtures were

ground in an agate mortar under acetone, loaded into graphite cassettes as a powder, and dried at 100°C for 12 hours.

The in situ XRD experiments were conducted at the SPing-8 synchrotron radiation facility (Japan), using a Kawai-cell and DIA-type press, "SPEED-MkII", installed at a bending magnet beam line BL04B1 (Katsura et al. 2004). The incident X-rays were collimated to form a thin beam with dimensions of 0.05 mm in the horizontal direction and 0.2 mm in the vertical direction by WC slits and directed to the sample through a boron-epoxy window in pyrophyllite gaskets and a MgO insert in the ZrO_2 PM. A Ge solid-state detector with a 4096 channel analyzer was used. The analyzer was calibrated by using characteristic x-rays of Cu, Mo, Ag, La, Ta, Pt, Au, and Pb. The diffraction angle was approximately 5.98°, calibrated before compression using the known *d*-values of XRD peaks of MgO, with an uncertainty of less than 0.0005°. The dimensions of the high-pressure cell and sample preparation procedure for the XRD experiments were the same as for the quenched experiments. The cell assembly contains two graphite cassettes. Each cassette contains three holes filled with carbonate mixtures. In the present paper we present XRD data from one of the six samples, namely K_2CO_3-$MgCO_3$ mixtures loaded in a lower middle hole (Fig. 1b and 4). Pressures were calculated from the Au and MgO unit cell volumes using equation of states (Dorogokupets and Dewaele 2007; Sokolova et al. 2013) with the temperature indicated by the thermocouple.

Study of post-experimental samples. The K_2CO_3-bearing samples are very hydroscopic and adsorb large amounts of water within minutes under atmosphere conditions. Therefore, a special care was taken to minimize the amount of time the samples are exposed to the air. Recovered samples were mounted into petro-epoxy and polished in low-viscosity oil using 400-, 1000- and 1500-mesh sandpapers and 3-

μm diamond past. The sample surface was cleaned using an oil spray between each step of polishing. The samples were always covered by a film of oil during polishing the sample surface, which was checked under binocular microscope. Finally we used petroleum Benzene to remove oil after polishing immediately prior to coating and loading the sample into a scanning electron microscope. Samples were studied using a JSM 5410 scanning electron microscope equipped with Oxford Instruments Link ISIS Series 300 energy-dispersive X-ray spectroscopic (EDS) microanalysis system at Tohoku University (Sendai, Japan). EDS spectra were collected by rastering the electron beam over a surface area available for the analysis with linear dimensions from 10 to 300 μm at 15 kV accelerating voltage and 10 nA load current. No beam damage or change in measured composition with time was observed at these settings. The correctness of the EDS measurements was confirmed under the same conditions using post-experimental samples with known compositions and homogeneous textures obtained below the solidus.

Experimental results

The system K_2CO_3-$MgCO_3$. Selected backscattered electron (BSE) images of sample cross-sections in the system K_2CO_3-$MgCO_3$ are shown in Figure 5. The subsolidus samples displayed homogeneous aggregates of carbonate phases with grain size varying from several micrometers to several tens of micrometers (Fig. 5a,d,e,g). In non-stoichiometric mixtures the limited reagents, i.e. $MgCO_3$ at $X(MgCO_3) \leq 40$ mol% (Fig. 5a) and K_2CO_3 at $X(MgCO_3) \geq 60$ mol% (Fig. 5e,g), have been consumed completely (Table 1). In stoichiometric mixture, $X(MgCO_3) = 50$ mol%, both reagents, K_2CO_3 and $MgCO_3$, were completely consumed to form $K_2Mg(CO_3)_2$ (Fig. 5d, Table

1). This suggests that reactions have gone to completion and equilibrium has been achieved.

A dome-shaped volume of carbonate crystals up to 500 μm in size in the cool region and a quenched melt segregated to the hot region were observed in the run products below the liquidus (Fig. 5b,c,f,h,i). Although at low pressure the K_2CO_3-$MgCO_3$ join is a well known glass-forming system (Data and Tuttle 1964), in our high-pressure experiments the melts quenched from 1400 to 200ºC with a rate of about 60°C/sec and formed dendritic aggregates rather than glass (Fig. 5b,c,f,h,i). The liquid-crystal interface has a rounded outline coinciding with the typical shape expected for an isotherm in a high-pressure cell (Fig. 3b, 5b,c,f,h,i). The formation of the dome-shaped interface has been discussed in our previous study (Shatskiy et al. 2010b).

Alkali-carbonate melts are known as very mobile and extremely reactive compounds which are difficult to seal in a high-pressure cell. To overcome this encapsulation problem we used tightly closed graphite capsules (Fig. 1a). Since our multicharge experiments also contained carbonate samples with different cation compositions such as Na-Ca, Na-Mg, or K-Ca, which in some cases were loaded into the same cassette, it was easy to monitor the performance of those capsules at given P-T conditions and run durations in terms of proper carbonate melt sealing. EDS analysis did not show any alien cations in our post-experimental samples.

Both K_2CO_3 and $K_2Mg(CO_3)_2$ melts are known as solvent catalysts for the graphite-to-diamond transformation (Taniguchi et al. 1996; Borzdov et al. 1999). Although our experiments were performed in the field of thermodynamic stability of diamond (Kennedy and Kennedy 1976), no diamonds were found in the run products even after sample annealing at 1400 ºC and 6 GPa for 6 hours. This is consistent with

previous results for the system K_2CO_3-C in which no diamonds appeared even after 40 hours at 5.7 GPa and 1420 °C (Pal'yanov et al. 1999a), while diamond nucleation was established at 6.3 GPa, 1650 °C with the same run duration (Shatskii et al. 2002). This can be explained by the long time required for diamond to nucleate in the K and Na carbonate systems, which diminishes with increasing temperature and pressure from ≥40 hours at 5.7 GPa and 1420 ºC to 20 minutes at 7 GPa and 1700-1750 ºC (Pal'yanov et al. 1999b).

Phase relations established in the system K_2CO_3-$MgCO_3$ at 6 GPa are illustrated in Figure 6. An intermediate phase, $K_2Mg(CO_3)_2$, was observed between 900 and 1200ºC in association with K_2CO_3 in the range of 10 – 40 mol% $MgCO_3$ (Fig. 5a) and in association with magnesite in the range of 60 – 90 mol% $MgCO_3$ (Fig. 5e,g). The first melt with nearly eutectic composition (~25 mol% $MgCO_3$) appeared at 1200ºC at $X(MgCO_3)$ < 50 mol% (Fig. 5b), whereas at $X(MgCO_3)$ > 50 mol% the first melt was formed at 1300ºC (Fig. 5f,h).

The K_2CO_3-$MgCO_3$ join has two eutectics: near 25 mol% $MgCO_3$ and 1200 ºC and near 52 mol% $MgSiO_3$ and 1250 ºC (Fig. 5, 6). As shown in Table 1, K_2CO_3 does not melt up to 1400 ºC. Melting of K_2CO_3 was established in additional run in the pure K_2CO_3 system at 1450 ºC. The established melting temperature at 6 GPa is about 250 ºC higher than that at 3.2 GPa reported by (Liu et al. 2006). Therefore, the flattening of K_2CO_3 melting curve reported by Liu et al. at 2.5 GPa ceases at higher pressure. This might occur due to the pressure induced phase transition.

Magnesite, whose melting temperature exceeds 1800ºC at 6 GPa (Katsura and Ito 1990), was observed in its subliquidus phase at 1300 ºC and $X(MgCO_3)$ > 50 mol%. Potassium solubility in magnesite does not exceed the detection limit of EDS employed in our study (i.e. <0.5 mol% K_2CO_3) (Table 1). In a recent study by Enggist

et al. (2012), authors employed a electron-microprobe analysis and reported the K_2CO_3 solubility in magnesite of about 0.04 mol% at 4-7 GPa and 1150-1200 °C in the system phlogopite-magnesite (90:10; wt%). Therefore, it is assumed that there is very little, if any, solid solution of K_2CO_3 in the $MgCO_3$ at 6 GPa.

The $K_2Mg(CO_3)_2$ phase remains in a solid state at 1200 ºC and melts congruently at 1300ºC (Fig. 6). A similar compound was also reported in a near solidus mineral assemblage in K-rich carbonated peridotite system at 6-10 GPa below 1400 ºC (Brey et al. 2011). This compound with space group $R\bar{3}m$ (Hesse and Simons 1982) was previously identified by X-ray diffraction in quenched products of carbonate, carbonate-silicate, and hydrous-carbonate-silicate melts recovered from 9-24 GPa and 1400-1750 ºC (Taniguchi et al. 1996; Shatskiy et al. 2007; Shatskiy et al. 2009). A $(K_{0.9\text{-}0.65}Na_{0.1\text{-}0.35})_2Mg(CO_3)_2$ compound with similar stoichiometry was also reported as a separate crystal phase above the solidus of alkaline carbonatite at 10-21 GPa (Litasov et al. 2013).

The system K_2CO_3-hydromagnesite. Phase relations established in the system K_2CO_3-hydromagnesite at 6 GPa are illustrated in Figures 7 and 8 and summarized in Table 2. A consecutive increase of hydromagnesite content in the system at 900 ºC leads to a change in the phase composition from K_2CO_3 + $K_2Mg(CO_3)_2$ assembly at 7 ≤ $X(MgCO_3)$ ≤ 19 mol% to $K_2Mg(CO_3)_2$ + liquid at 33 ≤ $X(MgCO_3)$ ≤ 42 mol% and magnesite + liquid/fluid at 52 ≤ $X(MgCO_3)$ ≤ 87 mol%, where $X(MgCO_3)=MgCO_3/(MgCO_3+K_2CO_3)$. The absence of liquid/fluid phase at $X(MgCO_3)$ ≤ 19 mol % suggests that K_2CO_3 can dissolve certain amount of water in its crystal structure at high-pressure (Fig. 7a). An additional spectroscopic study is needed to clarify this possibility. An increase in temperature to 1000 °C causes complete melting in the range of 19 ≤ $X(MgCO_3)$ ≤ 52 mol% and disappearance of the

$K_2Mg(CO_3)_2$ compound in the entire compositional range. Melts/fluids in equilibrium with magnesite have K–Mg carbonate compositions with $K_2CO_3/MgCO_3$ mole ratio up to 1.1 and shift with increasing hydromagnesite content toward hydrous-carbonate fluid or melt (Fig. 7g, 8).

The structure of $K_2Mg(CO_3)_2$. Although the $R\bar{3}m$ structure of the $K_2Mg(CO_3)_2$ compound recovered from HP-HT experiments has been confirmed in several studies, the *in situ* X-ray diffraction of this phase has yet to be reported. In the current study we collected several XRD patterns from the K-Mg carbonate mixture during sample heating to 1000°C at 6.5 GPa and decompression at room temperature down to 1 atmosphere. The experimental P-T pathway and obtained XRD patterns are shown in Figures 9 and 10. As can be seen, no major change in XRD patterns occurred during sample annealing and pressure decrease from 6.5 to 1.0 GPa. In addition to main peak all diffraction patterns contain a peak of graphite used as a sample capsule and peaks of magnesite. After the experiment, we confirmed by EDS that in addition to $K_2Mg(CO_3)_2$ the sample contains magnesite but does not contain K_2CO_3, which suggests a deviation of the starting mixture from $K_2Mg(CO_3)_2$ stoichiometry rather than a kinetic problem. Remaining peaks, including the most intense one, should be attributed to the $K_2Mg(CO_3)_2$ compound. Moreover, those peaks shift in the same manner with temperature and pressure. Yet, the positions of those peaks are different from the K-Mg carbonate with $R\bar{3}m$ structure (Hesse and Simons 1982). The combination of those peaks remained even after sample heating to 400 ºC at 1.3 GPa. However, these peaks disappeared after sample decompression at room temperature to 1 atmosphere. The last XRD pattern taken at ambient conditions exhibits peaks of the $K_2Mg(CO_3)_2$ compound with known $R\bar{3}m$ structure (Hesse and Simons 1982). Consequently, another polymorph of K-Mg carbonate would be stable at pressure

ranging from 1 to 6.5 GPa. The X-ray diffraction patterns were analyzed using "PDIndexer" software developed by Y.Seto (Seto et al. 2010). To determine crystal lattice parameters and autoindex diffraction pattern, we chose five definite peaks of the new polymorph (Fig. 10). For this set of data there is only one chemically plausible model showing a good fit with obtained patterns – orthorombic system with lattice parameters shown in Table 3. The unit cell volume of this phase is nearly 10% less than that of lower pressure polymorph.

Discussion

The water-bearing silicate phases, phlogopite and K-amphibole, are major storage sites for K in the Earth's upper mantle under hydrous conditions (Konzett and Fei 2000; Harlow and Davies 2004; Sobolev et al. 2009; Enggist et al. 2012). On the other hand, K-wadeite ($K_2Si_4O_9$) and phase X ($K_2Mg_2Si_2O_7$) were reported to be stable at 6-16 and 8-23 GPa, respectively, under "dry" conditions (Kanzaki et al. 1998; Shatskii et al. 2002; Harlow and Davies 2004; Shatskiy et al. 2009; Matsuzaki et al. 2010; Brey et al. 2011). Although K-wadeite can not be important for the peridotite mantle because it is not stable in an ultramafic environment, phase X can be a potential host for K in peridotite mantle (Harlow and Davies 2004; Brey et al. 2011). The stability field of phase X in the carbonated peridotite environment, however, is restricted by near solidus temperatures, whereas the stability field of the $K_2Mg(CO_3)_2$ is up to 200 °C wider (Brey et al. 2011). According to the present experimental results and recent data (Brey et al. 2011; Litasov et al. 2013), $K_2Mg(CO_3)_2$ could be a potential host phase of K in cold oxidized domains of the upper and lower mantle (e.g. subducted slabs) under anhydrous conditions. Assuming a typical mantle C and K abundances of 100 ppm and 260 ppm, respectively (Palme and O'Neill 2003), and

assuming all K and C form carbonates, the average contents of $K_2Mg(CO_3)_2$ and $MgCO_3$ in the oxidized mantle domains are estimated to be 740 and 141 ppm, respectively. This phase assemblage could control the solidus temperature of the carbonated mantle under "dry" conditions and cause formation of the ultrapotassic carbonatite melts similar to those found as microinclusions in "fibrous" diamonds (with 15-24 wt% K_2O and 17-28 wt% MgO) (Klein-BenDavid et al. 2007; Klein-BenDavid et al. 2009).

Although some carbonatitic melts in sublithospheric mantle were essentially anhydrous (e.g. parental melt of Udachnaya-Earst kimberlite (Kamenetsky et al. 2004; 2012)), the carbonate/(carbonate+water) molar ratio of the K- and Mg-rich hydrous carbonatite melt/fluid in diamond inclusions ranges from 0.5 to 0.7 indicating that measurable amounts of water are generally present in diamond forming carbonatitic melts (Klein-BenDavid et al. 2007). On the basis of obtained experimental results such melts could be formed as a result of partial melting of $K_2Mg(CO_3)_2$ and $MgCO_3$ bearing mineral assemblage in presence of water at 900-1000 ºC.

Acknowledgements

We are grateful to Dan Frost, Marc Hirschmann, Daniel Harlow and an anonymous reviewer for thorough reviews and useful suggestions and Jennifer Kung, Keith Putirka and Ian Swainson for editorial handling, telling criticism and comments. The synchrotron radiation experiments were performed at the BL04B1 in SPring-8 with the approval of the Japan Synchrotron Radiation Research Institute (JASRI) (proposals Nos. 2010B1308, 2011B1416, 2011B1163, and 2012B1548). This study was conducted as a part of the Global Center-of-Excellence program at Tohoku University. This work was also supported by the Ministry of education and science of

Russia (project No. 14.B37.21.0601) and by the Russian Foundation for Basic Research (project Nos. 12-05-01167 and 12-05-33008).

References cited

Bohlen, S.R., and Boettcher, A.L. (1982) The quartz+coesite transformation: A precise determination and the effects of other components. journal of Geophysical Research, 87, 7073-7078.

Borzdov, Y.M., Sokol, A.G., Pal'yanov, Y.N., Kalinin, A.A., and Sobolev, N.V. (1999) Studies of diamond crystallization in alkaline silicate, carbonate and carbonate-silicate melts. Doklady Akademii Nauk, 366(4), 530-533.

Brey, G.P., and Kohler, T. (1990) Geothermobarometry in Four-phase Lherzolites II. New Thermobarometers, and Practical Assessment of Existing Thermobarometers. Journal of Petrology, 31(6), 1353-1378.

Brey, G.P., Bulatov, V.K., and Girnis, A.V. (2011) Melting of K-rich carbonated peridotite at 6-10 GPa and the stability of K-phases in the upper mantle. Chemical Geology, 281(3-4), 333-342.

Data, R.K., and Tuttle, O.F. (1964) The preparation, properties and structure of carbonate glasses, p. AT(30-1)-2887. Rept. Atom. Ener. Comm., USA.

Decker, D.L., Bassett, W.A., Merrill, L., Hall, H.T., and Barnett, J.D. (1972) High-pressure calibration a critical review. J. Phys. Chem. Ref. Data. , 1, 1-79.

Dobretsov, N.L., and Shatskiy, A.F. (2012) Deep carbon cycle and geodynamics: the role of the core and carbonatite melts in the lower mantle. Russian Geology and Geophysics, 53, 1117-1132.

Dorogokupets, P.I., and Dewaele, A. (2007) Equations of state of MgO, au, pt, NaCl-B1, and NaCl-B2: Internally consistent high-temperature pressure scales. High Pressure Research, 27(4), 431-446.

Eitel, W., and Skaliks, W. (1929) Some double carbonates of alkali and earth alkali. Zeitschrift Fur Anorganische Und Allgemeine Chemie, 183(3), 263-286.

Enggist, A., Chu, L.L., and Luth, R.W. (2012) Phase relations of phlogopite with magnesite from 4 to 8 GPa. Contributions to Mineralogy and Petrology, 163(3), 467-481.

Genge, M.J., Jones, A.P., and Price, G.D. (1995) An infrared and Raman-study of carbonate glasses - implications for the structure of carbonatite magmas. Geochimica Et Cosmochimica Acta, 59(5), 927-937.

Golovin, A.V., Sharygin, V.V., and Pokhilenko, N.P. (2007) Melt inclusions in olivine phenocrysts in unaltered kimberlites from the Udachnaya-East pipe, Yakutia: Some aspects of kimberlite magma evolution during late crystallization stages. Petrology, 15(2), 168-183.

Grassi, D., and Schmidt, M.W. (2011) The Melting of Carbonated Pelites from 70 to 700 km Depth. Journal of Petrology, 52(4), 765-789.

Green, D.H., and Wallace, M.E. (1988) Mantle metasomatism by ephemeral carbonatite melts. Nature, 336(6198), 459-462.

Haggerty, S.E. (1989) Mantle metasomes and the kinship between carbonatites and kimberlites. In K. Bell, Ed. Carbonatites: Genesis and Evolution, p. 546-560. Unwin Hyman Ltd, London.

Harlow, G.E. (1997) K in clinopyroxene at high pressure and temperature: An experimental study. American Mineralogist, 82(3-4), 259-269.

Harlow, G.E., and Veblen, D.R. (1991) Potassium in clinopyroxene inclusions from diamonds. Science, 251(4994), 652-655.

Harlow, G.E., and Davies, R. (2004) Status report on stability of K-rich phases at mantle conditions. Lithos, 77, 647-653.

Haygarth, J.C., Getting, I.C., and Kennedy, G.C. (1967) Determination of the Pressure of the Barium I-II Transition with Single-Stage Piston-Cylinder Apparatus Journal of Applied Physics, 38(12), 4557.

Hernlund, J., Leinenweber, K., Locke, D., and Tyburczy, J.A. (2006) A numerical model for steady-state temperature distributions in solid-medium high-pressure cell assemblies. American Mineralogist, 91(2-3), 295-305.

Hesse, K.-F., and Simons, B. (1982) Crystalstructure of synthetic $K_2Mg(CO_3)_2$. Zeitschrift fur Kristallographie, 161, 289-292.

Izraeli, E.S., Harris, J.W., and Navon, O. (2004) Fluid and mineral inclusions in cloudy diamonds from Koffiefontein, South Africa. Geochimica et Cosmochimica Acta, 68, 2561–2575.

Kamenetsky, M.B., Sobolev, A.V., Kamenetsky, V.S., Maas, R., Danyushevsky, L.V., Thomas, R., Pokhilenko, N.P., and Sobolev, N.V. (2004) Kimberlite melts rich in alkali chlorides and carbonates: A potent metasomatic agent in the mantle. Geology, 32(10), 845-848.

Kamenetsky, V.S., Kamenetsky, M.B., Weiss, Y., Navon, O., Nielsen, T.F.D., and Mernagh, T.P. (2009) How unique is the Udachnaya-East kimberlite? Comparison with kimberlites from the Slave Craton (Canada) and SW Greenland. Lithos, 112, 334-346.

Kamenetsky, V.S., Kamenetsky, M.B., Golovin, A.V., Sharygin, V.V., and Maas, R. (2012) Ultrafresh salty kimberlite of the Udachnaya-East pipe (Yakutia, Russia): A petrological oddity or fortuitous discovery? Lithos, 152, 173-186.

Kanzaki, M., Xue, X.Y., and Stebbins, J.F. (1998) Phase relations in Na_2O-SiO_2 and $K_2Si_4O_9$ systems up to 14 GPa and Si-29 NMR study of the new high-pressure phases: implications to the structure of high-pressure silicate glasses. Physics of the Earth and Planetary Interiors, 107(1-3), 9-21.

Katsura, T., and Ito, E. (1990) Melting and subsolidus relations in the $MgSiO_3$–$MgCO_3$ system at high pressures: implications to evolution of the Earth's atmosphere. Earth and Planetary Science Letters, 99, 110–117.

Katsura, T., Funakoshi, K., Kubo, A., Nishiyama, N., Tange, Y., Sueda, Y., Kubo, T., and Utsumi, W. (2004) A large-volume high-pressure and high-temperature apparatus for in situ X-ray observation, 'SPEED-Mk.II'. Physics of the Earth and Planetary Interiors, 143, 497-506.

Kennedy, C.S., and Kennedy, G.C. (1976) The equilibrium boundary between graphite and diamond. Journal of Geophysical Research, 81(14), 2467-2470.

Klein-BenDavid, O., Izraeli, E.S., Hauri, E., and Navon, O. (2007) Fluid inclusions in diamonds from the Diavik mine, Canada and the evolution of diamond-forming fluids. Geochimica Et Cosmochimica Acta, 71(3), 723-744.

Klein-BenDavid, O., Logvinova, A.M., Schrauder, M., Spetius, Z.V., Weiss, Y., Hauri, E.H., Kaminsky, F.V., Sobolev, N.V., and Navon, O. (2009) High-Mg carbonatitic microinclusions in some Yakutian diamonds-a new type of diamond-forming fluid. Lithos, 112, 648-659.

Konzett, J., and Fei, Y.W. (2000) Transport and storage of potassium in the Earth's upper mantle and transition zone: an experimental study to 23 GPa in simplified and natural bulk compositions. Journal of Petrology, 41(4), 583-603.

Korsakov, A.V., Golovin, A.V., De Gussem, K., Sharygin, I.S., and Vandenabeele, P. (2009) First finding of burkeite in melt inclusions in olivine from sheared lherzolite xenoliths. Spectrochimica Acta Part A: Molecular and Biomolecular Spectroscopy, 73(3), 424-427.

Litasov, K.D. (2011) Physicochemical conditions for melting in the Earth's mantle containing a C–O–H fluid (from experimental data). Russian Geology and Geophysics, 52, 475-492.

Litasov, K.D., Shatskiy, A., Ohtani, E., and Yaxley, G.M. (2013) The Solidus of Alkaline Carbonatite in the Deep Mantle. Geology, 41(1), 79-82.

Litasov, K.D., Sharygin, I.S., Shatskiy, A.F., Ohtani, E., and Pokhilenko, N.P. (2010) Experimental Constraints on the Role of Chloride in the Origin and Evolution of Kimberlitic Magma. Doklady Earth Sciences, 435(2), 1641-1646.

Liu, Q., Tenner, T.J., and Lange, R.A. (2006) Do carbonate liquids become denser than silicate liquids at pressure? Constraints from the fusion curve of K_2CO_3 to 3.2 GPa. Contributions to Mineralogy and Petrology, 153, 55-66.

Lloyd, E.C., Johnson, D.P., and Hutton, U.O. (1963) Dual-wedge high-pressure appaeatus. Unated States Patent, 3,100,912.

Logvinova, A.M., Wirth, R., Tomilenko, A.A., Afanas'ev, V.P., and Sobolev, N.V. (2011) The phase composition of crystal-fluid nanoinclusions in alluvial diamonds in the northeastern Siberian Platform. Russian Geology and Geophysics, 52, 1286-1297.

Malinovskii, I.Y., Shurin, Y.I., and Ran, E.N. (1989). Phase transformation at high pressures and high temperatures: Applications to geophysical and petrological problems, Misasa, Tottori - ken, Japan.

Matsuzaki, T., Hagiya, K., Shatskiy, A., Katsura, T., and Matsui, M. (2010) Crystal structure of anhydrous phase X, $K_{1.93}(Mg_{2.02}Cr_{0.02})Si_{2.00}O_7$. Journal of Mineralogical and Petrological Sciences, 105(6), 303-308.

Navon, O. (1991) High internal pressure in diamond fluid inclusions determined by infrared absorption. Nature, 353(6346), 746-748.

Ono, S., Kikegawa, T., and Higo, Y. (2011) In situ observation of a garnet/perovskite transition in $CaGeO_3$. Physics and Chemistry of Minerals, 38, 735-740.

Osugi, J., Shimizu, K., Inoue, K., and Yasunami, K. (1964) A compact cubic anvil high pressure apparatus. Review of Physical Chemistry of Japan, 34(1), 1-6.

Palme, H., and O'Neill, H.S.C. (2003) Cosmochemical estimates of mantle composition. In A.M. Davis, H.D. Holland, and K.K. Turekian, Eds. Treatise on geochemistry, v.2. Elsevier. 1-38.

Pal'yanov, Y.N., Sokol, A.G., Borzdov, Y.M., Khokhryakov, A.F., and Sobolev, N.V. (1999a) Diamond formation from mantle carbonate fluids. Nature, 400(6743), 417-418.

Pal'yanov, Y.N., Sokol, A.G., Borzdov, Y.M., Khokhryakov, A.F., and Sobolev, N.V. (2002) Diamond formation through carbonate-silicate interaction. American Mineralogist, 87(7), 1009-1013.

Pal'yanov, Y.N., Sokol, A.G., Borzdov, Y.M., Khokhryakov, A.F., Shatsky, A.F., and Sobolev, N.V. (1999b) The diamond growth from Li_2CO_3, Na_2CO_3, K_2CO_3 and Cs_2CO_3 solvent-catalysts at P=7 GPa and T=1700-1750 ^oC. Diamond and Related Materials, 8(6), 1118-1124.

Palyanov, Y.N., Shatsky, V.S., Sobolev, N.V., and Sokol, A.G. (2007) The role of mantle ultrapotassic fluids in diamond formation. Proceedings of the National Academy of Sciences of the United States of America, 104(22), 9122-9127.

Palyanov, Y.N., Borzdov, Y.M., Khokhryakov, A.F., Kupriyanov, I.N., and Sokol, A.G. (2010) Effect of Nitrogen Impurity on Diamond Crystal Growth Processes. Crystal Growth & Design, 10(7), 3169-3175.

Palyanov, Y.N., Malinovskii, I.Y., Borzdov, Y.M., Khokhryakov, A.F., Chepurov, A.I., Godovikov, A.A., and Sobolev, N.V. (1990) Growing of large diamond crystals in press-free split-sphere type apparatus. Doklady Akademii Nauk SSSR, 315(5), 1221-1224.

Ragone, S.E., Datta, R.K., Roy, D.M., and Tuttle, O.F. (1966) The System Potassium Carbonate-Magnesium Carbonate. Journal of Physical Chemistry, 70(10), 3360-3361.

Schrauder, M., and Navon, O. (1994) Hydrous and carbonatitic mantle fluids in fibrous diamonds from Jwaneng, Botswana. Geochimica Et Cosmochimica Acta, 58(2), 761-771.

Seto, Y., Nishio-Hamane, D., Nagai, T., and Sata, N. (2010) Development of a Software Suite on X-ray Diffraction Experiments. The Review of High Pressure Science and Technology, 20, 269-276.

Sharma, S.K., and Simons, B. (1980) Raman study of K_2CO_3-$MgCO_3$ glasses. Carnegie Inst Washington Yearb, 79, 322-326.

Sharygin, I.S., Litasov, K.D., Shatskiy, A.F., Golovin, A.V., Ohtani, E., and Pokhilenko, N.P. (2013) Melting of kimberlite of the Udachnaya East pipe: experimental study at 3–6.5 GPa and 900–1500°C. Doklady Earth Sciences, 448, 200-205.

Sharygin, I.S., Korsakov, A.V., Golovin, A.V., and Pokhilenko, N.P. (2013) Eitelite from Udachanya-East kimberlite pipe (Russia) – A new locality and host rock type. European Journal of Mineralogy, in press.

Shatskii, A.F., Borzdov, Y.M., Sokol, A.G., and Pal'yanov, Y.N. (2002) Phase formation and diamond crystallization in carbon-bearing ultrapotassic carbonate-silicate systems. Geologiya I Geofizika, 43(10), 940-950.

Shatskiy, A., Litasov, K.D., Terasaki, H., Katsura, T., and Ohtani, E. (2010a) Performance of semi-sintered ceramics as pressure-transmitting media up to 30GPa. High Pressure Research, 30(3), 443-450.

Shatskiy, A., Fukui, H., Matsuzaki, T., Shinoda, K., Yoneda, A., Yamazaki, D., Ito, E., and Katsura, T. (2007) Growth of large (1 mm) $MgSiO_3$ perovskite single crystals: A thermal gradient method at ultrahigh pressure. American Mineralogist, 92(10), 1744-1749.

Shatskiy, A., Litasov, K.D., Matsuzaki, T., Shinoda, K., Yamazaki, D., Yoneda, A., Ito, E., and Katsura, T. (2009) Single crystal growth of wadsleyite. American Mineralogist, 94(8-9), 1130-1136.

Shatskiy, A., Yamazaki, D., Borzdov, Y.M., Matsuzaki, T., Litasov, K.D., Cooray, T., Ferot, A., Ito, E., and Katsura, T. (2010b) Stishovite single-crystal growth and application to silicon self-diffusion measurements. American Mineralogist, 95(1), 135-143.

Shatskiy, A., Katsura, T., Litasov, K.D., Shcherbakova, A.V., Borzdov, Y.M., Yamazaki, D., Yoneda, A., Ohtani, E., and Ito, E. (2011) High pressure generation using scaled-up Kawai-cell. Physics of the Earth and Planetary Interiors, 189(1-2), 92-108.

Shatsky, V., Ragozin, A., Zedgenizov, D., and Mityukhin, S. (2008) Evidence for multistage evolution in a xenolith of diamond-bearing eclogite from the Udachnaya kimberlite pipe. Lithos, 105(3-4), 289-300.

Shatsky, V.S., Sobolev, N.V., and Vavilov, M.A. (1995) Diamond-bearing metamorphic rocks from the Kokchetav massif (Northern Kazakhstan). In R.G. Coleman, and X. Wang, Eds. Ultrahigh Pressure Metamorphism, p. 427-455. Cambridge University Press.

Simons, B., and Sharma, S.K. (1982) Structures of glasses in the system K_2CO_3-$MgCO_3$ EOS, 63, 469-470.

Sobolev, N.V., and Shatsky, V.S. (1990) Diamond inclusions in garnets from metamorfic rocks: a new environment for diamond formation. Nature, 343(6260), 742-746.

Sobolev, N.V., Logvinova, A.M., and Efimova, E.S. (2009) Syngenetic phlogopite inclusions in kimberlite-hosted diamonds: implications for role of volatiles in diamond formation. Russian Geology and Geophysics, 50(12), 1234-1248.

Sobolev, N.V., Bakumenko, I.T., Yefimova, E.S., and Pokhilenko, N.P. (1991) Peculiarities of microdiamond morphology, sodium content in garnets and potassium content in pyroxenes of 2 eclogite xenoliths from the Udachnaya kimberlite pipe (Yakutia). Doklady Akademii Nauk Sssr, 321(3), 585-592.

Sobolev, V.S., Sobolev, N.V., and Lavrent'yev, Y.G. (1972) Inclusions in diamond from diamondiferous eclogite. Doklady Akademii Nauk SSSR, 207, 164-167.

Sokolova, E.V., Dorogokupets, P.I., and Litasov, K.D. (2013) Self-consistent pressure scales based on the equations of state for ruby, diamond, MgO, B2-NaCl, as well as Au, Pt and other metals to 4 Mbars and 3000 K. Russian Geology and Geophysics, 54(2), 181-199.

Sweeney, R.J. (1994) Carbonatite melt compositions in the Earth's mantle. Earth and Planetary Science Letters, 128(3-4), 259-270.

Taniguchi, T., Dobson, D., Jones, A.P., Rabe, R., and Milledge, H.J. (1996) Synthesis of cubic diamond in the graphite-magnesium carbonate and graphite-$K_2Mg(CO_3)_2$ systems at high pressure of 9–10 GPa region. Journal of Materials Research, 11, 2622-2632.

Tomlinson, E.L., Jones, A.P., and Harris, J.W. (2006) Co-existing fluid and silicate inclusions in mantle diamond. Earth and Planetary Science Letters, 250(3-4), 581-595.

Wallace, M.E., and Green, D.H. (1988) An experimental determination of primary carbonatite magma composition. Nature, 335(6188), 343-346.

Weiss, Y., Kessel, R., Griffin, W.L., Kiflawi, I., Klein-BenDavid, O., Bell, D.R., Harris, J.W., and Navon, O. (2009) A new model for the evolution of diamond-forming fluids: Evidence from microinclusion-bearing diamonds from Kankan, Guinea. Lithos, 112, 660-674.

Yaxley, G.M., Crawford, A.J., and Green, D.H. (1991) Evidence for carbonatite metasomatism in spinel peridotite xenoliths from western Victoria, Australia. Earth and Planetary Science Letters, 107(2), 305-317.

Zedgenizov, D.A., Ragozin, A.L., Shatsky, V.S., Araujo, D., and Griffin, W.L. (2011) Fibrous diamonds from the placers of the northeastern Siberian Platform: carbonate and silicate crystallization media. Russian Geology and Geophysics, 52(11), 1298-1309.

Zedgenizov, D.A., Ragozin, A.L., Shatsky, V.S., Araujo, D., Griffin, W.L., and Kagi, H. (2009) Mg and Fe-rich carbonate-silicate high-density fluids in cuboid

diamonds from the Internationalnaya kimberlite pipe (Yakutia). Lithos, 112, 638-647.

Table 1. Compositions (in mol% K_2CO_3) of the run products in the system K_2CO_3-$MgCO_3$ at 6 GPa.

Run, T, τ	Run Product	$X(K_2CO_3)$ in the system, mol% 90	75	60	50	40	30	20	10
ES346	K_2CO_3	100.0[a]	×	×	×	–	–	–	–
1400ºC	$K_2Mg(CO_3)_2$	–	×	×	×	–	–	–	–
6 h	$MgCO_3$	–	×	×	×	–	0.0	0.1	0.1
	Liquid	–	×	×	×	41.1	35.0	36.3(8)	33.5(8)
T2020	K_2CO_3	99.5	–	–	–	–	–	–	–
1300ºC	$K_2Mg(CO_3)_2$	–	–	–	–	–	–	–	–
4 h	$MgCO_3$	–	–	–	–	0.3	0.1	0.0	0.0
	Liquid	84.7(1.2)	73.5(7)	59.8	48.4	43.6	45.2(1)	42.6(5)	43.9(9)
ES342	K_2CO_3	100.1	99.9(02)	100.0(9)	–	–	–	–	–
1200ºC	$K_2Mg(CO_3)_2$	50.2	50.7	49.8	50.0	51.0	50.5	50.7	50.2
12 h	$MgCO_3$	–	–	–	–	0.0	0.1	0.1	0.2
	Liquid	75.5(2)	72.8(9)	70.8(1.0)	–	–	–	–	–
ES347	K_2CO_3	98.6(1.9)	99.2(8)	100.1	–	–	–	–	–
1150ºC	$K_2Mg(CO_3)_2$	51.0	49.8	50.7	49.3	50.7	50.3	49.2	47.9(1.5)
18 h	$MgCO_3$	–	–	–	–	0.2	0.2	0.3	0.0
	Liquid	–	–	–	–	–	–	–	–
T2022	K_2CO_3	100.1(5)	99.4	99.8	–	–	–	–	–
1100ºC	$K_2Mg(CO_3)_2$	49.8	49.9	51.6	50.5	51.4	49.2(1.)	50.2(2)	49.8
16 h	$MgCO_3$	–	–	–	–	0.2	0.1(01)	0.1	–0.1
	Liquid	–	–	–	–	–	–	–	–
ES343	K_2CO_3	100.1	99.8	100.2	–	–	–	–	–
1000ºC	$K_2Mg(CO_3)_2$	50.5	49.8	50.6	49.1	48.8	50.9	47.7	50.1
19 h	$MgCO_3$	–	–	–	–	0.2	0.1	0.2	0.0
	Liquid	–	–	–	–	–	–	–	–
T2021	K_2CO_3	97.8	100.0	100.1	–	–	–	–	–
900ºC	$K_2Mg(CO_3)_2$	50.4	50.1	49.7	51.3	50.0	49.4	51.1	51.9
43 h	$MgCO_3$	–	–	–	–	0.2	0.0	0.2	0.1
	Liquid	–	–	–	–	–	–	–	–

Note: [a] – It is pure K_2CO_3 system; τ – run duration; × – no data. Standard deviations are given in parentheses, where the number of measurement is more than one. Letters in the run number, ES and T denote the type of press, wedge and DIA, respectively.

Table 2. Conditions and results of experiments in the system K_2CO_3-hydromagnesite at 6 GPa.

Run		Initial compositions, $MgCO_3/K_2CO_3/H_2O$, mol%							
T, τ	Phases	7/89/4	17/73/10	28/57/15	31/52/17	34/47/19	40/37/23	46/28/26	58/9/33
1002/1, 1000°C, 30 h.	K_2CO_3[a]	97.8	–	–	–	×	–	–	–
	$MgCO_3$[a]	–	–	–	–	×	0.2	0.1(1)	0.1(1)
Liquid	Mole fract.	<0.1	1*	1*	1*	×	0.94(3)	0.80(7)	0.50(14)
Liquid	$MgCO_3$	×	17	28	31	×	38.8(7)	41.0(2.3)	41.2(8.2)
Liquid	K_2CO_3	×	73	57	52	×	38.2(5)	30.4(1.2)	12.7(1.8)
Liquid	H_2O	×	10	15	17	×	23.0(3)	28.6(1.1)	46.0(6.4)
1001/1, 900°C, 38 h.	K_2CO_3[a]	99.7	99.9(5)	–	–	–	–	–	–
	$K_2Mg(CO_3)_2$[a]	49.7(1.2)	49.7(1.5)	49.8(8)	50.8(7)	49.3(1.1)	–	–	–
	$MgCO_3$[a]	–	–	–	–	–	0.1(2)	0.4	0.1
Liquid	Mole fract.	0	0	×	0.4(1)	0.50(7)	0.87(7)	0.65(7)	0.3(1)
Liquid	$MgCO_3$	–	–	×	19.5(3.7)	25.7(1.6)	37.0(2.0)	36.1(2.5)	29.6(8.7)
Liquid	K_2CO_3	–	–	×	53.3(4)	45.6(3)	39.3(1.2)	33.0(1.3)	15.2(1.9)
Liquid	H_2O	–	–	×	27.2(3.3)	28.7(1.9)	23.7(7)	31.0(1.2)	55.1(6.8)

Note: [a] – composition is given in mol% K_2CO_3; (–) – no phase; × – no data; τ – run duration. Standard deviations are given in parentheses, wherever the number of measurement is more than one. CO_2 and H_2O contents in the liquid were calculated from mass balance using the compositions of starting material and analyses of phases..

Table 3. Lattice parameters of orthorhombic $K_2Mg(CO_3)_2$. Volumes are in Å 3 , pressures are in GPa.

T, °C	V_{Au}	P_{Au}	V_{MgO}	P_{MgO}	*a*	*b*	*c*	*V*
500	66.67(1)	6.37(4)	73.30(3)	5.93(7)	8.7600(6)	7.7764(7)	4.9684(5)	338.45(3)
500	–//–	–//–	–//–	–//–	8.7642(6)	7.7760(7)	4.9737(5)	338.96(3)
800	67.39(3)	6.57(8)	73.91(2)	6.39(5)	8.8355(6)	7.8365(7)	5.0158(5)	347.29(4)
1000	67.98(2)	6.54(5)	74.43(2)	6.50(5)	8.8898(7)	7.8673(7)	5.0528(5)	353.39(4)
55	67.28(3)	4.39(8)	72.65(12)	4.90(30)	8.7837(6)	7.8246(7)	4.9774(5)	342.09(4)
27	66.74(5)	2.90(14)	73.34(2)	3.09(5)	8.8569(6)	7.8480(7)	5.0211(5)	349.02(4)
27	67.49(3)	0.92(8)	74.21(2)	1.10(4)	8.8885(7)	8.0555(8)	5.0783(6)	363.62(4)
27	67.40(3)	1.15(8)	74.18(2)	1.17(5)	9.0235(7)	8.0148(8)	5.1259(6)	370.71(4)

Figure 1. Kawai-type cell assembly employed to study phase relations in carbonate systems at 6 GPa using a uniaxial press with DIA- and wedge-type guide blocks. (a) Cell design employed in quenched experiments at 900-1450 °C. (b) Cell design used in X-ray diffraction experiments at 27-1000 °C. The K_2CO_3-$MgCO_3$ mixture was loaded in a lower middle hole. Dimensions are in millimeters.

Figure 2. Pressure calibration curves for ZrO_2 high-pressure cell (PM edge length 20.5 mm, TEL 12.0 mm, and pyrophyllite gaskets, 4 mm in width and thickness) compressed by the wedge- and DIA-type apparatuses. Qz – quartz, Co – coesite, Grt – garnet, Pv – perovskite.

Figure 3. Temperature distribution along the sample chamber in the Kawai-type high-pressure cell with 20.5 mm edge length of ZrO_2 PM and TEL = 12 mm. (a) Results of sample chamber mapping using the two-pyroxene thermometer (Brey and Kohler 1990). The average temperatures and standard deviation are shown at the left side of the figure. The obtained data do not show systematical temperature change in horizontal (radial) direction. (b) The sample chamber examined by the thermal modeling software (Hernlund et al. 2006). An upper-left square encloses a modeled assembly area at 900 and 1400 ºC. Isotherms through the sample charge and adjacent assembly parts overlie the cartoon.

Figure 4. Radiographic image of sample charge before compression (a) and that under press load of 6 MN, corresponding to the sample pressure of about 6 GPa (b) (run # M1250).

Figure 5. Representative BSE images of sample cross-sections illustrating phase relations in the systems K_2CO_3-$MgCO_3$ at 6 GPa. K_2 = K_2CO_3; K_2Mg = $K_2Mg(CO_3)_2$; Mgst = $MgCO_3$; L = quenched liquid. Gravity vector is directed from right to left in each image. High-temperature side is located at the left side of each image.

Figure 6. Phase relations in K_2CO_3-$MgCO_3$ system at 6 GPa. K_2 = K_2CO_3; K_2Mg = $K_2Mg(CO_3)_2$; Mgst = $MgCO_3$; L = liquid. Grey circles mark melt composition measured by EDS. Grey areas in circles denote phases observed in lower temperature side of partially molten samples.

Figure 7. Representative BSE images of sample cross-sections illustrating phase relations in the systems K_2CO_3-hydromagnesite at 6 GPa. K_{2SS} = H_2O and/or $MgCO_3$ solid-solutions in K_2CO_3; K_2Mg = $K_2Mg(CO_3)_2$; Mgst = $MgCO_3$; L = quenched liquid or fluid. Gravity vector is directed from right to left in each image. The cassettes with samples were placed in the center of a sample charge of a BARS cell, where axial thermal gradient is negligibly small. Therefore, melt segregates in accordance with radial thermal gradient.

Figure 8. Ternary diagrams illustrating the water effect on melting phase relations in the K_2CO_3-$MgCO_3$ system at 6 GPa and 1000 °C (a) and 900 ºC (b).

Figure 9. P-T pathway of the run M1250 on the *in situ* X-ray diffraction study of $K_2Mg(CO_3)_2$. Grey circles with numbers above denote the conditions at which X-ray data from the sample were collected.

Figure 10. Representative diffraction profiles of K_2CO_3-$MgCO_3$ sample in the run M1250. (a) A new orthorhombic polymorph of $K_2Mg(CO_3)_2$ was established during sample heating up to 1000 °C at pressure exceeding 6 GPa. (b) During decompression the new polymorph persists to at least 1 GPa. (c) Recovered $K_2Mg(CO_3)_2$ exhibits a trigonal $R\bar{3}m$ structure previously established at ambient conditions.

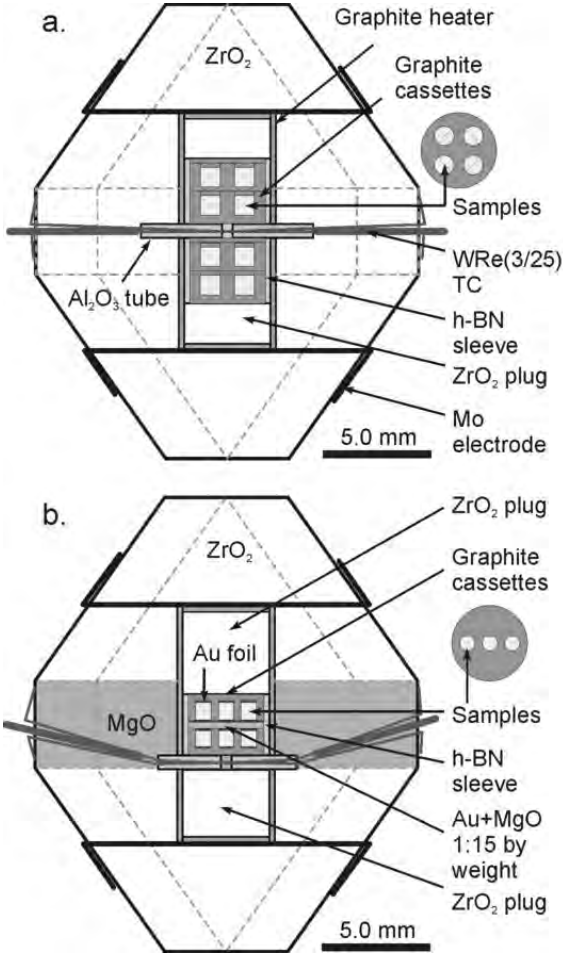
a.
Graphite heater
ZrO_2
Graphite cassettes
Samples
WRe(3/25) TC
Al_2O_3 tube
h-BN sleeve
ZrO_2 plug
Mo electrode
5.0 mm
b.
ZrO_2 plug
ZrO_2
Graphite cassettes
Au foil
MgO
Samples
h-BN sleeve
Au+MgO 1:15 by weight
ZrO_2 plug
5.0 mm

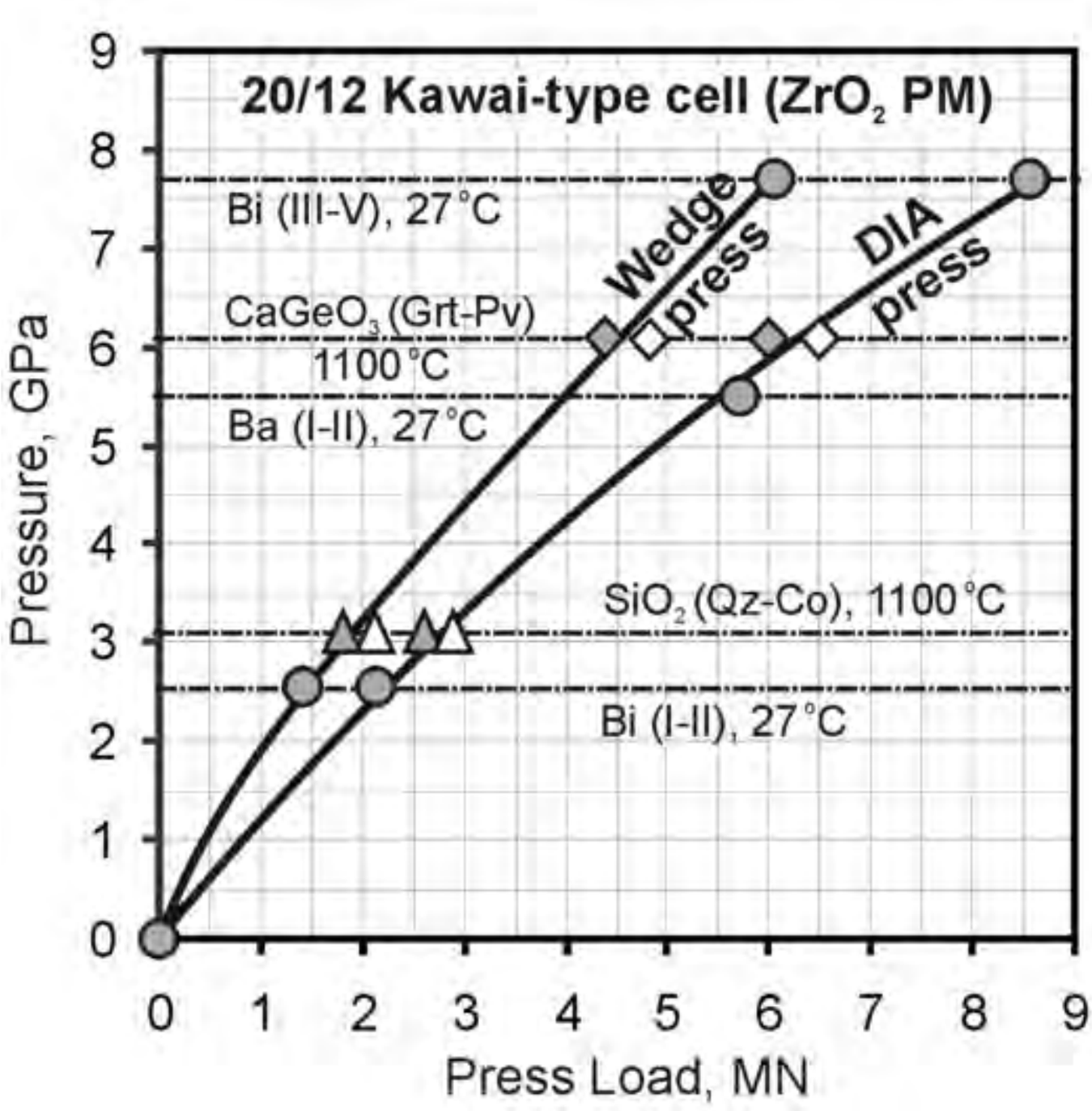
20/12 Kawai-type cell (ZrO_2 PM)
Bi (III-V), 27 °C
$CaGeO_3$ (Grt-Pv)
1100 °C
Ba (I-II), 27 °C
SiO_2 (Qz-Co), 1100 °C
Bi (I-II), 27 °C
Wedge press
DIA press
Pressure, GPa
Press Load, MN
0
1
2
3
4
5
6
7
8
9

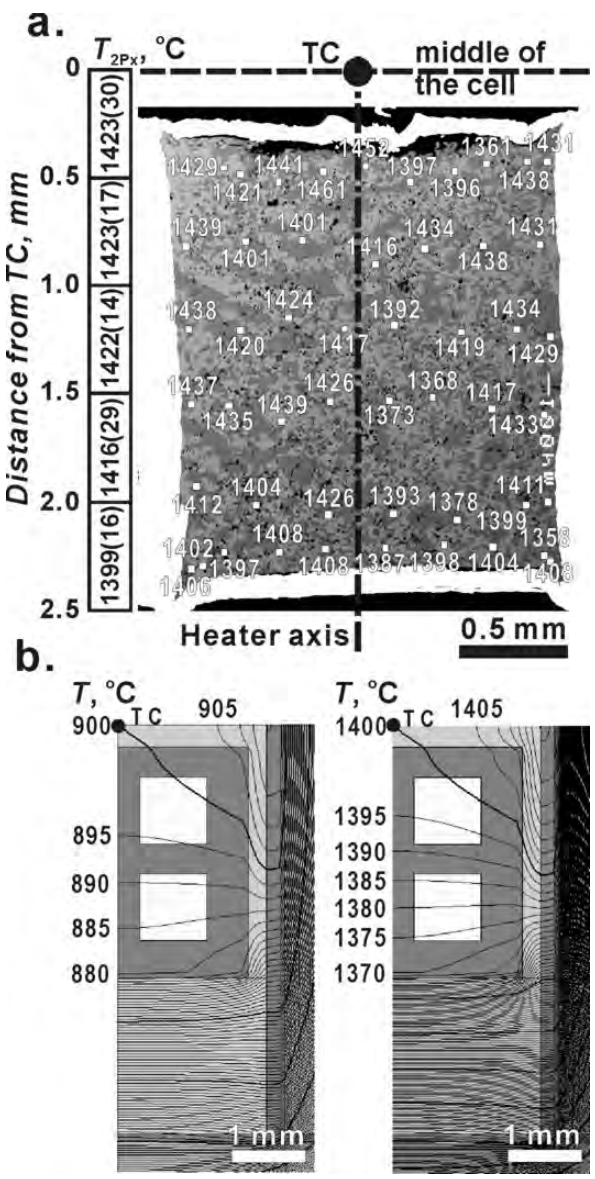
a.
T_{2Px}, °C
TC
middle of the cell
0
0.5
1.0
1.5
2.0
2.5
Distance from TC, mm
1423(30)
1423(17)
1422(14)
1416(29)
1399(16)
Heater axis
0.5 mm
b.
T, °C
TC
905
900
895
890
885
880
1 mm
T, °C
TC
1405
1400
1395
1390
1385
1380
1375
1370
1 mm

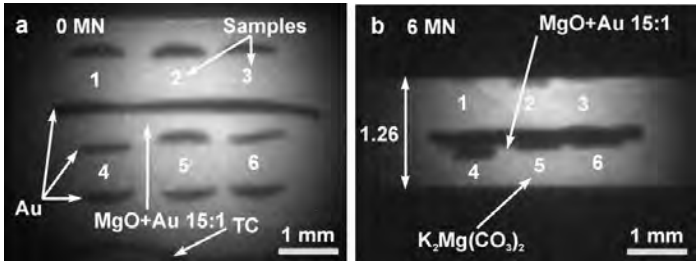
a
0 MN
Samples
1
2
3
4
5
6
Au
MgO+Au 15:1
TC
1 mm
b
6 MN
MgO+Au 15:1
1.26
1
2
3
4
5
6
K2Mg(CO3)2
1 mm

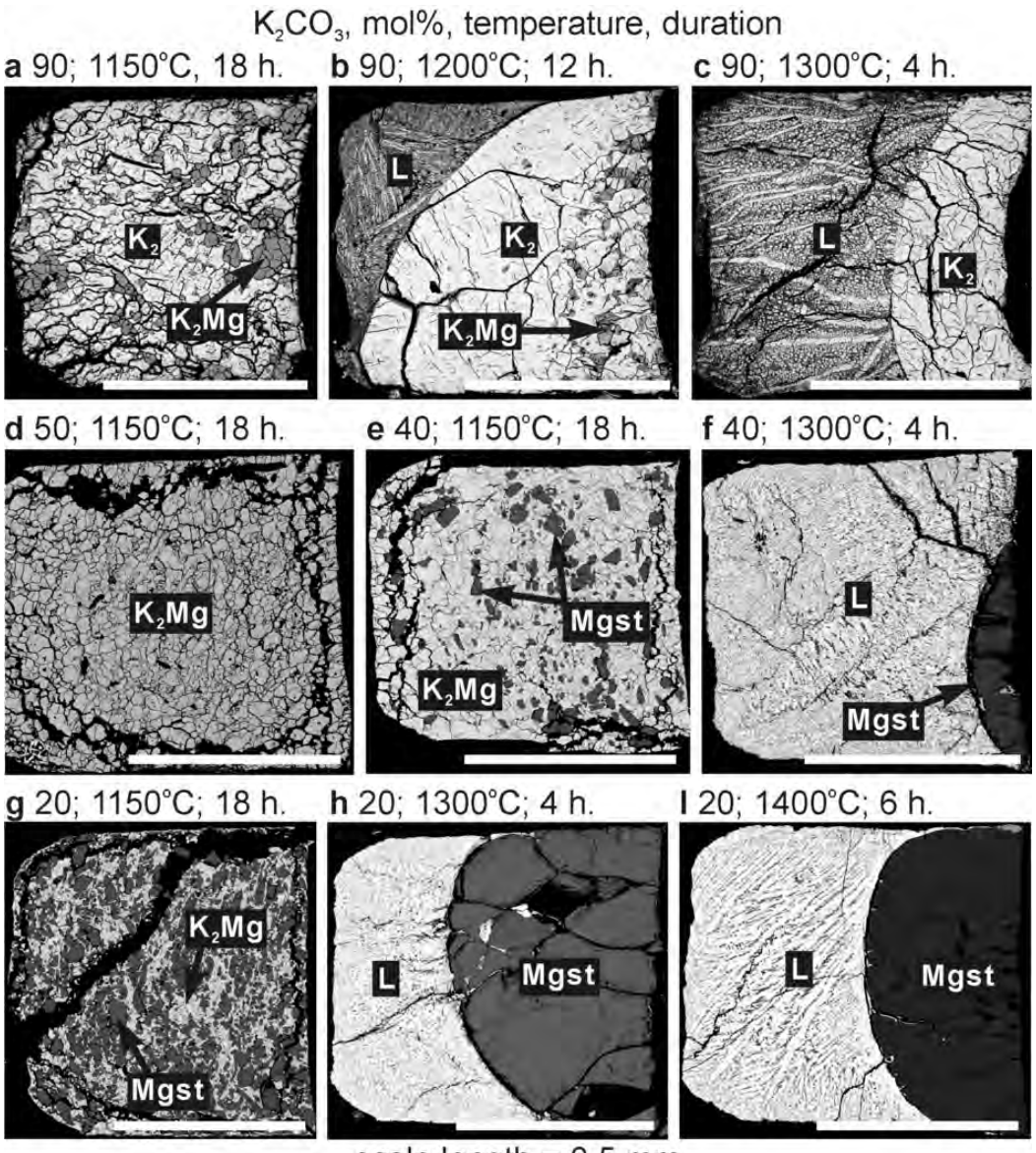
K_2CO_3, mol%, temperature, duration
a 90; 1150°C, 18 h.
b 90; 1200°C; 12 h.
c 90; 1300°C; 4 h.
K_2
K_2Mg
L
K_2
K_2Mg
L
K_2
d 50; 1150°C; 18 h.
e 40; 1150°C; 18 h.
f 40; 1300°C; 4 h.
K_2Mg
Mgst
K_2Mg
L
Mgst
g 20; 1150°C; 18 h.
h 20; 1300°C; 4 h.
I 20; 1400°C; 6 h.
K_2Mg
Mgst
L
Mgst
L
Mgst
scale length = 0.5 mm

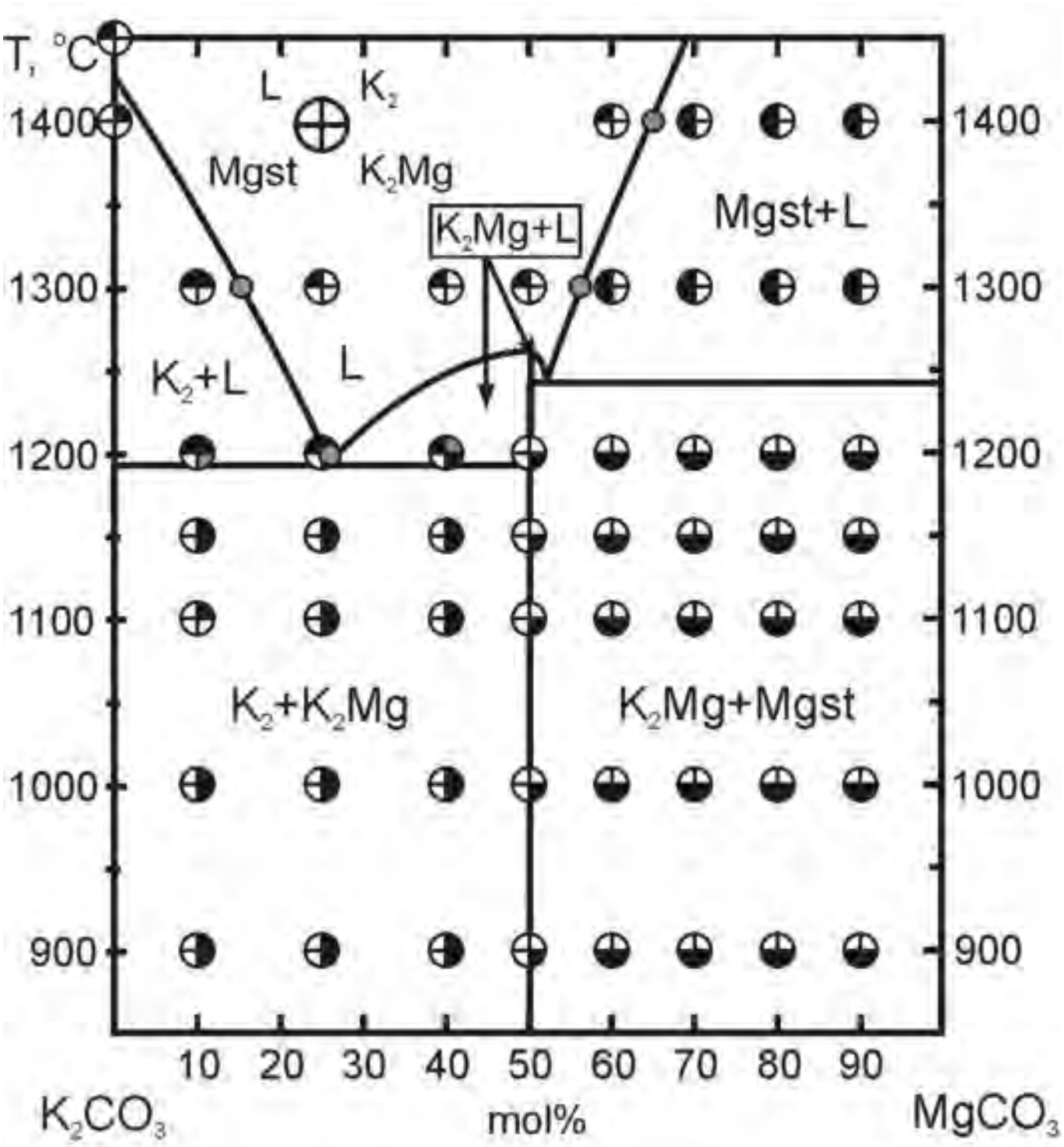
T, °C
1400
1300
1200
1100
1000
900
L
K2
Mgst
K2Mg
K2Mg+L
Mgst+L
K2+L
L
K2+K2Mg
K2Mg+Mgst
10 20 30 40 50 60 70 80 90
K2CO3
mol%
MgCO3

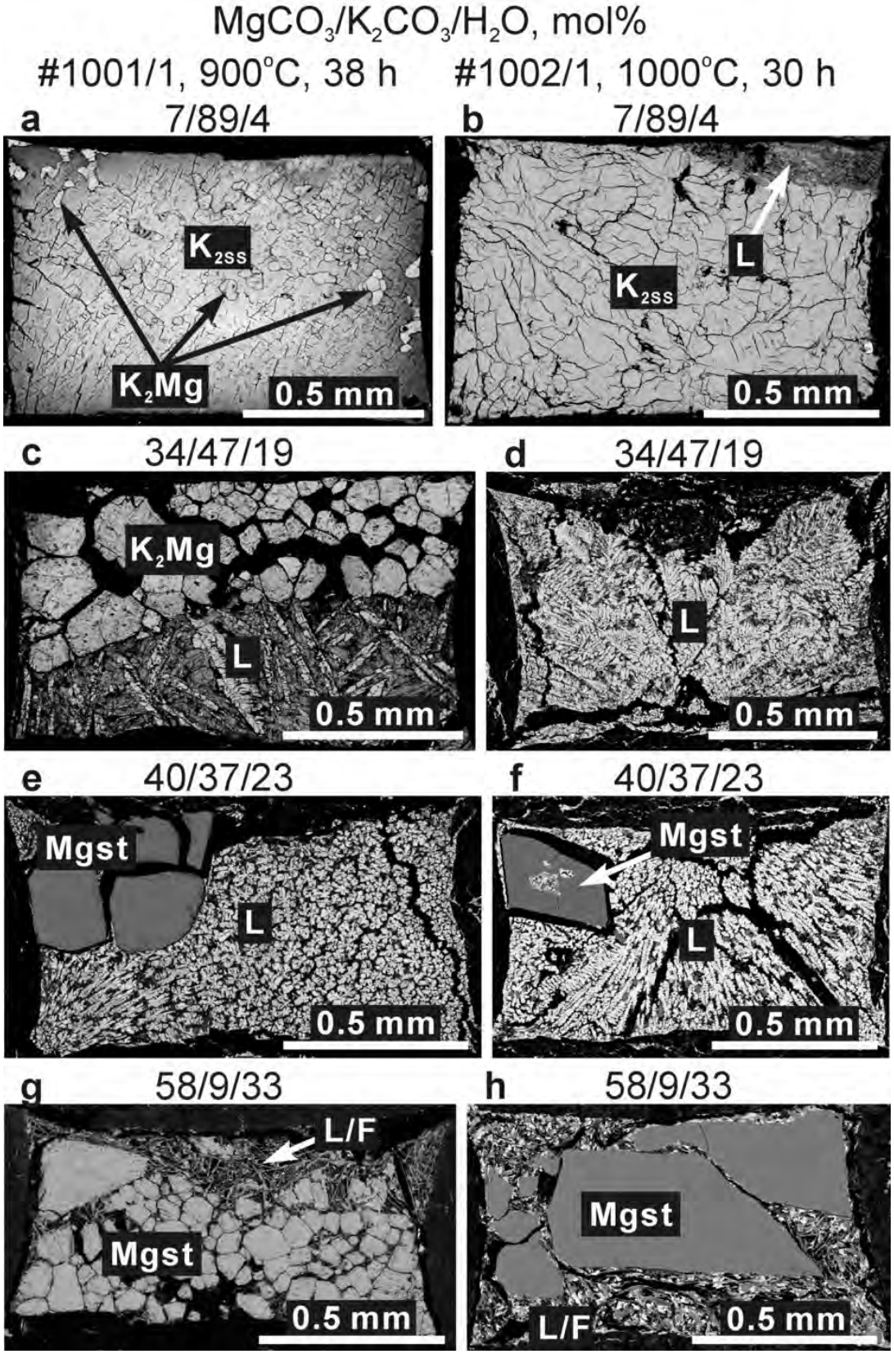
MgCO3/K2CO3/H2O, mol%
#1001/1, 900°C, 38 h
#1002/1, 1000°C, 30 h
a
7/89/4
K2ss
K2Mg
0.5 mm
b
7/89/4
L
K2ss
0.5 mm
c
34/47/19
K2Mg
L
0.5 mm
d
34/47/19
L
0.5 mm
e
40/37/23
Mgst
L
0.5 mm
f
40/37/23
Mgst
L
0.5 mm
g
58/9/33
L/F
Mgst
0.5 mm
h
58/9/33
Mgst
L/F
0.5 mm

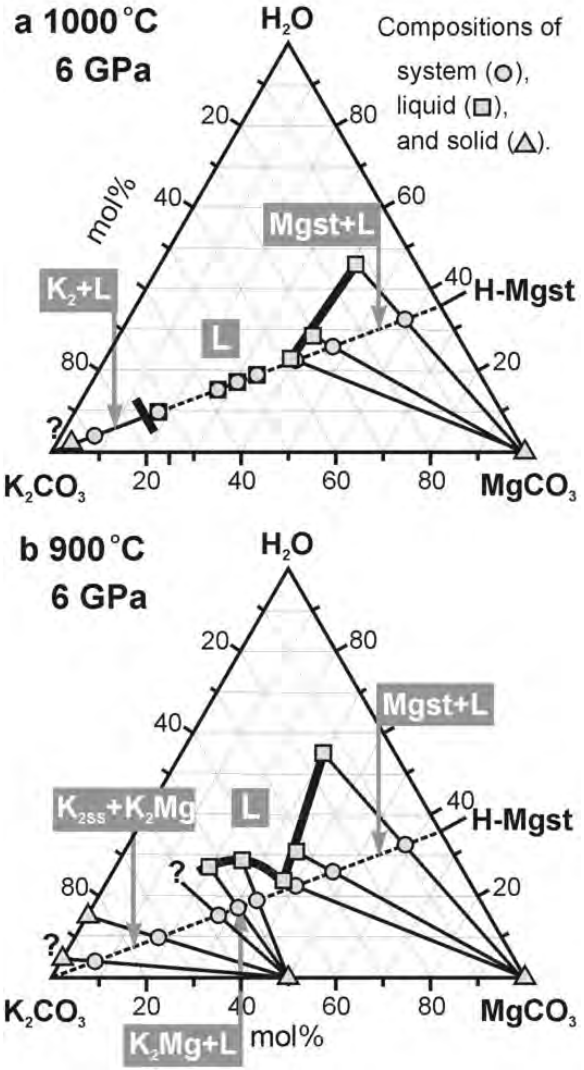
a 1000 °C
6 GPa
H2O
Compositions of system (○), liquid (□), and solid (△).
mol%
Mgst+L
K2+L
L
H-Mgst
?
K2CO3
MgCO3
b 900 °C
6 GPa
H2O
Mgst+L
K2ss+K2Mg
L
H-Mgst
?
K2CO3
K2Mg+L
mol%
MgCO3

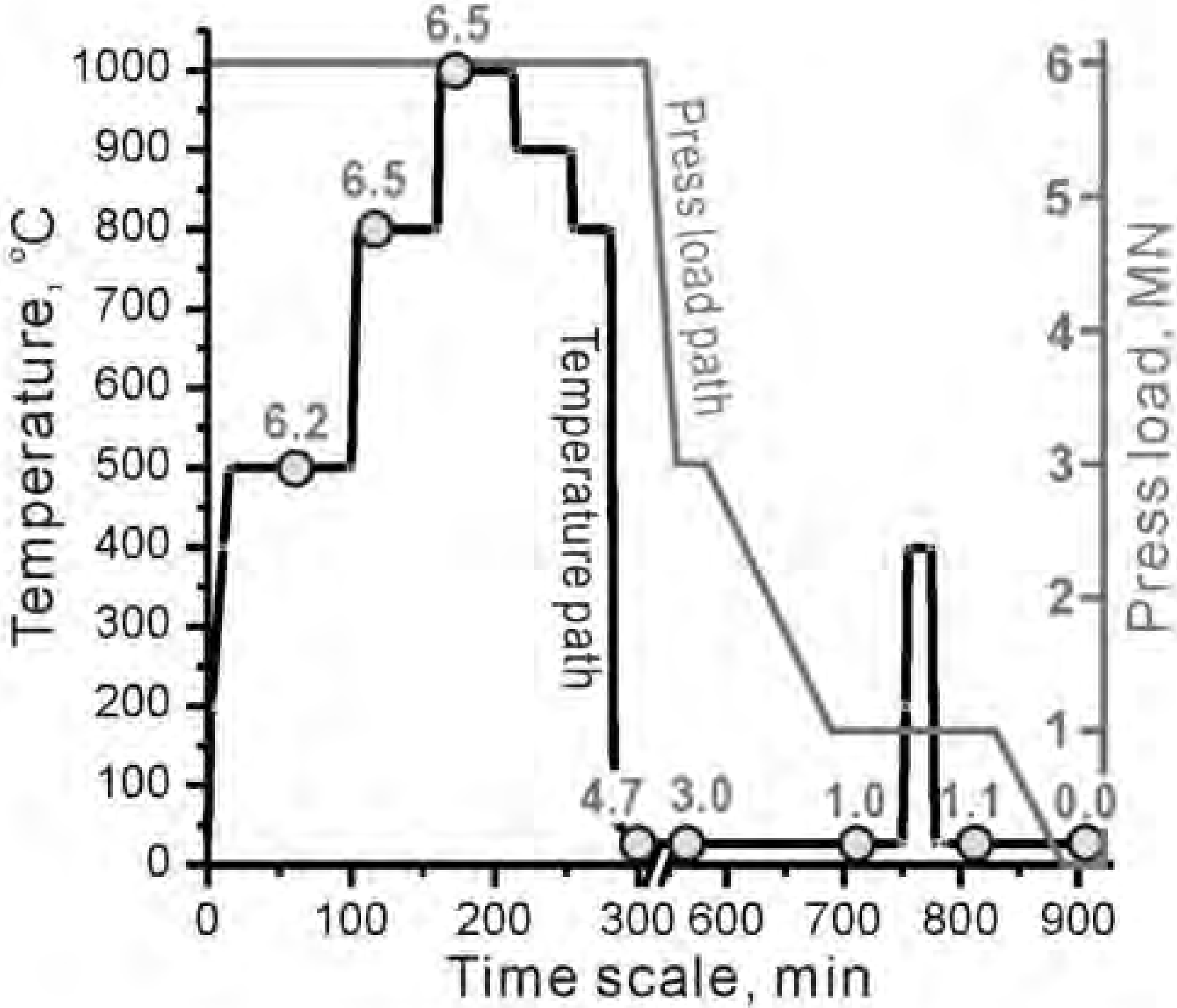
Temperature, °C
1000
900
800
700
600
500
400
300
200
100
0
Press load, MN
6
5
4
3
2
1
0
0
100
200
300
600
700
800
900
Time scale, min
Temperature path
Press load path
6.5
6.5
6.2
4.7
3.0
1.0
1.1
0.0

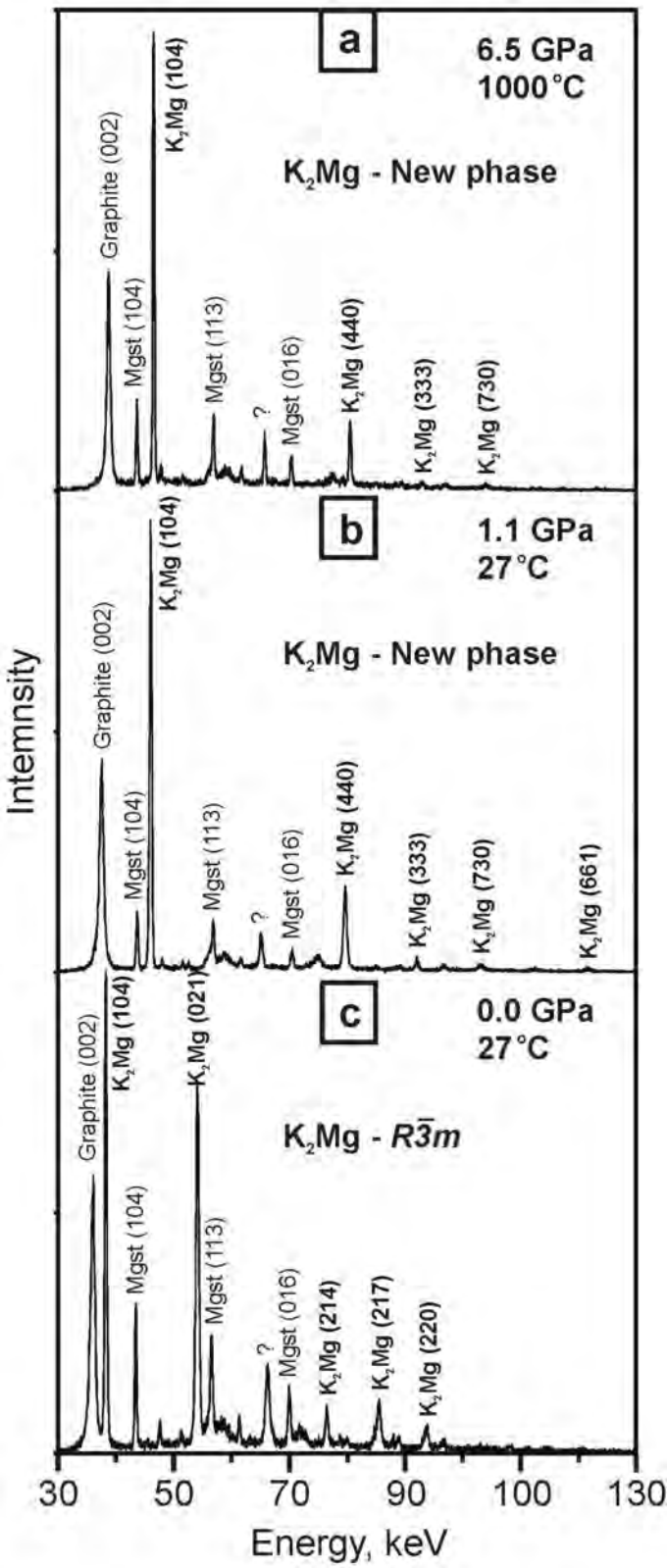
a
6.5 GPa
1000°C
K2Mg - New phase
Graphite (002)
Mgst (104)
K2Mg (104)
Mgst (113)
?
Mgst (016)
K2Mg (440)
K2Mg (333)
K2Mg (730)
b
1.1 GPa
27°C
K2Mg - New phase
Graphite (002)
Mgst (104)
K2Mg (104)
Mgst (113)
?
Mgst (016)
K2Mg (440)
K2Mg (333)
K2Mg (730)
K2Mg (661)
c
0.0 GPa
27°C
K2Mg - R3̄m
Graphite (002)
K2Mg (104)
Mgst (104)
K2Mg (021)
Mgst (113)
?
Mgst (016)
K2Mg (214)
K2Mg (217)
K2Mg (220)
Intemnsity
30
50
70
90
100
130
Energy, keV